

N 62 63056

RM L54L02a

CASE FILE
COPY



NACA

RESEARCH MEMORANDUM

ANALYSIS OF AERODYNAMIC BLADE-LOADING-LIMIT PARAMETERS

FOR NACA 65- $(C_{l_0} A_{10})$ 10 COMPRESSOR-BLADE

SECTIONS AT LOW SPEEDS

By Melvyn Savage

Langley Aeronautical Laboratory
Langley Field, Va.

NATIONAL ADVISORY COMMITTEE
FOR AERONAUTICS

WASHINGTON

April 25, 1955

Declassified October 14, 1957

NATIONAL ADVISORY COMMITTEE FOR AERONAUTICS

RESEARCH MEMORANDUM

ANALYSIS OF AERODYNAMIC BLADE-LOADING-LIMIT PARAMETERS

FOR NACA 65- $(C_{l_0} A_{10})_{10}$ COMPRESSOR-BLADE

SECTIONS AT LOW SPEEDS

By Melvyn Savage

SUMMARY

A simple cascade loading-limit parameter for incompressible axial-flow compressor-blade elements was developed from an analysis of published incompressible-flow cascade and rotor data on the NACA 65- $(C_{l_0} A_{10})_{10}$ blade sections. The loading-limit parameter was evaluated from blade-surface-measured pressure distributions. It is the ratio of the suction surface maximum static-pressure rise to the difference between the stagnation and static pressures at the point of maximum surface velocity and is herein referred to as the C-factor.

Analysis of incompressible cascade test data over a range of isolated airfoil lift coefficients from 0.4 to 1.8, inlet angles from 30° to 70° , and solidities from 0.50 to 1.50 indicated that the loading limit for low-loss operation was approximately 0.70. At values of the loading-limit parameter from 0.75 to 0.80, the drag coefficient had increased significantly.

Analysis of incompressible rotor test data over a wide range of inlet-angle and solidity conditions indicated that at the mean radius station the trend of loss-coefficient variation with C-factor was approximately the same as that in the cascade data for the variation of drag coefficient with C-factor. At both the inboard and outboard rotor stations, loss coefficient increased more rapidly with C-factor than it did at the mean radius.

For the rotor conditions examined in this report, C-factor appeared to be effective in estimating rotor stall. The region of rotor stall was defined by a narrow range of C-factors, evaluated at the radial station where rotor stall was first initiated, for a wide range of inlet-angle conditions at each solidity. (C = 0.75 to over 0.78 at a solidity of 1.0 and 0.70 to 0.74 at a solidity of 0.5.)

The incompressible rotor data were also examined by utilizing the D-factor (blade-section diffusion factor) of NACA RM E53D01. Good agreement was obtained between the limiting value of design-angle-of-attack D-factor proposed in that paper ($D = 0.60$) and that obtained from the rotor data analyzed herein at the mean radius station. The results herein obtained, however, did indicate lower limits at the inboard station and a less rapid increase in loss with design-angle-of-attack D-factor at the outboard station than the D-factor report indicated. The use of the D-factor to correlate losses or as a loading limit for low-loss operation should be restricted to conditions near design angle of attack, as might be expected since D-factor was derived for design-angle-of-attack conditions. Nevertheless, the rotor tests analyzed herein did indicate that D-factor appeared to be effective as a rotor-stall indicator for rotor stall initiated in the tip region.

INTRODUCTION

One of the general methods of designing axial-flow compressors is to calculate velocity diagrams for the various stages and utilize cascade or rotor data to select blade sections, solidities, and blade-setting angles. In the original velocity-diagram computations and blade selections, however, some loading-limit criteria which define the region where severe flow separation occurs must be used to ensure satisfactory design and off-design performance. The loading-limit criteria used prior to the publication of reference 1 were generally very conservative empirical rules that various designers had used successfully. The present requirements for compressors of high-stage pressure ratio require that compressor-blade elements work near the actual aerodynamic loading limits; therefore, loading-limit criteria that more closely predict the actual aerodynamic loading limit are needed. One step toward the development of an effective loading-limit parameter was presented in reference 1 and was derived by utilizing an approximate relation between a separation criterion used in two-dimensional incompressible turbulent-boundary-layer theory and the external velocity diagram and solidity of the blade element. The approximation was facilitated through the use of the two-dimensional low-speed cascade data of reference 2 at design angle of attack. Test results for several rotors and stators were analyzed by using this limit parameter called the D-factor. It was shown that the D-factor was effective as a limit parameter at design angle of attack for inlet Mach numbers up to critical speed for both NACA 65-series and circular-arc-type blade sections for conditions similar to those of the several rotors and stators analyzed.

The purpose of this investigation is to establish a loading-limit parameter which is a measure of the blade loading at all angles of attack and, hence, is not restricted to design-angle-of-attack conditions. Blade surface pressures determine whether flow separation occurs. Hence, the establishment of a blade-loading limit parameter which would eventually

be applicable to both incompressible- and compressible-flow conditions for any type of blading must reflect the pressure-distribution shape. The present analysis is restricted to incompressible flow. The loading-limit parameter used is based on a separation criteria similar to that used for isolated airfoils (ref. 3). The parameter is defined as the ratio of the suction surface maximum static-pressure rise to the difference between the stagnation and static pressures at the point of maximum surface velocity. It is evaluated by using low-speed cascade and rotor data for the NACA 65-($C_{l_0} A_{10}$)10 compressor-blade sections (refs. 2 and 4).

The low-speed rotor data were also used to provide a comparative evaluation of the effectiveness of the C- and D-factors as loading limits over the wide range of cascade parameters of these data.

SYMBOLS

Many of the symbols given are illustrated in figure 1.

C	blade-section loading parameter defined as $\frac{\Delta p}{P - p_p}$ and equal to $\frac{\Delta p}{q_p}$ for incompressible flow
C_{l_0}	blade-section camber (the isolated airfoil lift coefficient)
C_{d_1}	section drag coefficient
D	blade-section diffusion factor defined as $1 - \frac{V_{2,r}}{V_{1,r}} + \frac{\Delta V_\theta}{2\sigma V_{1,r}}$
P	stagnation pressure, lb/ft ²
p	static pressure, lb/ft ²
Δp	maximum pressure rise on blade suction surface, lb/ft ²
q	dynamic pressure, lb/ft ²
U	rotational speed of rotor, ft/sec
V	velocity, ft/sec
ΔV_θ	change in tangential velocity across a blade row, ft/sec

α	angle of attack, deg
β	flow angle measured from axial direction, deg
σ	solidity (ratio of blade chord to blade spacing)
ξ	blade-setting angle measured from axial direction, deg
\bar{w}	loss coefficient, $\frac{P_{2,r,i} - P_{2,r}}{P_{i,r} - P_1}$

Subscripts:

a	axial
d	design-angle-of-attack condition
i	ideal
m	mean radius section of rotor
p	peak surface-velocity point on blade
r	relative to rotating blade
1	upstream of blade row
2	downstream of blade row

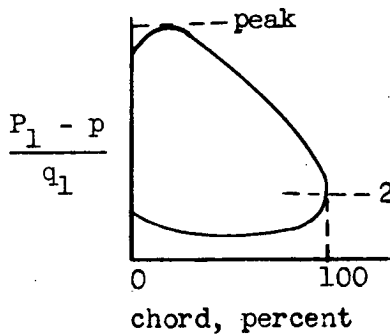
ANALYSIS OF LOW-SPEED CASCADE DATA TO DETERMINE
LOADING-LIMIT PARAMETER

Method of Approach

The loading limit for compressor-blade sections is defined as the blade loading above which high loss coefficients occur. High loss coefficient results as a direct consequence of flow separation of the blade boundary layer. Hence, the determination of a loading limit is really analogous to determining the conditions under which boundary-layer separation occurs. The growth and separation of the blade boundary layer is dependent on the blade-surface pressure distributions which in turn are dependent on solidity, inlet angle, angle of attack, relative inlet Mach number, and on blade-surface shape as affected by camber and thickness. Since the problem of predicting the occurrence of boundary-layer separation by analytical means is very difficult, it was considered

advisable to examine approximate methods of estimating the occurrence of boundary-layer separation. For angles of attack at and above design, it is the suction surface pressures which predominantly govern the blade boundary-layer growth and hence separation. It was shown by Loftin and Von Doenhoff (ref. 3) that, for isolated airfoils, separation corresponding to the occurrence of the maximum lift coefficient of various airfoils occurred at a relatively constant value of the ratio of the difference between the minimum static pressure near the leading edge and the static pressure at the 95-percent-chord point to the maximum dynamic pressure. This result is reasonable since the results of Von Doenhoff and Tetervin (ref. 5) indicated that, for the same boundary-layer shape at the start of the adverse gradient, the separation of the turbulent boundary layer is primarily related to the amount of static-pressure recovery and is only secondarily dependent on the detailed shape of the pressure distribution.

A similar approach to the prediction of flow separation was undertaken for airfoils in cascade by utilizing the low-speed cascade data for the NACA 65-series blades presented in reference 2. The pressure-recovery parameter, computed from the cascade pressure distributions and herein called C-factor, was similar to that used in reference 3. The parameter used is defined as the ratio of the maximum suction-surface static-pressure rise to the difference between the stagnation and static pressure at the point of maximum surface velocity; hence, the parameter is equal to $\frac{\Delta p}{q_p}$, where Δp and q_p are indicated in the following sketch of a typical low-speed cascade pressure distribution:



with

$$\Delta p = \left[\left(\frac{P_1 - p}{q_1} \right)_{\text{peak}} - \left(\frac{P_1 - p}{q_1} \right)_2 \right] q_1 \quad \text{and} \quad q_p = \left(\frac{P_1 - p}{q_1} \right)_{\text{peak}} q_1$$

The effectiveness of such a parameter in estimating the occurrence of flow separation for airfoils in cascade will be determined by noting how effectively the parameter correlates cascade drag and rotor-loss-coefficient data independent of the various cascade parameters, namely, inlet angle, solidity, camber, and angle of attack.

The C-factor differs from the D-factor of reference 1 since C-factor presumes that suction-surface boundary-layer growth and separation are predominantly governed by the magnitude of the maximum pressure recovery on the suction surface, whereas the D-factor presumes that the predominant parameter is the maximum velocity change on that surface; that is,

$$C = \frac{\Delta p}{P - p_p}$$

$$D \propto \frac{V_p - V_2}{V_{av}}$$

where V_{av} is some average surface velocity between V_p and V_2 . An evaluation of C-factor requires a knowledge of the minimum pressure on the suction surface, whereas the velocity-change term in the foregoing D-factor expression has been approximated at design angle of attack in reference 1 so that D-factor may be evaluated without recourse to blade surface pressures.

Evaluation of C-factor at Twice Minimum Drag

for Low-Speed Cascade Data

Howell's stall criterion (ref. 6) in which blade stall is defined as occurring at twice minimum drag was arbitrarily selected as a limiting condition. For this limiting condition, the C-factor was evaluated from low-speed cascade data (most of which are presented in ref. 2) for the NACA 65-series $C_{l_0} = 0.4, 1.2, \text{ and } 1.8$ blades at angles of β ranging from 30° to 70° and values of σ from 0.5 to 1.5. (See fig. 2.) The solidity 0.50 and 0.75 data were all obtained by using $2\frac{1}{2}$ -inch-chord blades at test Reynolds numbers from 175,000 to 220,000. The Reynolds number for all tests at the other solidities was 245,000 and the chord length was 5 inches. All drag data obtained from reference 1 were faired to eliminate irregular dips which eliminated all minimum drag values below 0.010. Some scatter in the C-factor is to be expected because the peak surface velocity could occur somewhere between the finite number of orifices used to measure surface pressures.

Figure 2 indicates that a limiting C-factor range from about 0.75 to 0.80 describes the region of twice minimum drag for inlet angles from 30° to 70° , solidities from 0.50 to 1.5, and cambers from 0.4 to 1.8 except for the 0.4 camber section at solidities from 0.88 to 0.50 where a gradual drop in C-factor level from 0.75 to 0.70 occurs. One possible explanation for the reduction in C-factor with solidity at constant C_{l_0} is that as solidity decreases the peak velocity may actually

be closer to the nose than the foremost pressure orifices could measure, resulting in a higher C-factor than is calculated. The C-factor was effective in describing the region of twice minimum drag since a narrow range of C-factors (0.75 to 0.80) described the region of twice minimum drag for a wide range of camber, inlet angle, and solidity conditions with the exception of the $C_{l_0} = 0.4$ blade at the low solidity conditions.

Hence, the C-factor appeared to be usable as a limit-loading parameter. Since the selection of twice minimum drag is a rather arbitrary limit selection when considering how minimum drag varies with loading, it was considered advisable to examine the C-factor over the entire drag range for all cambers for which test data were available.

Variation of Low-Speed Cascade Drag Coefficient

With C-Factor

The variation in C_{d1} with C-factor for design angle of attack and above for values of C_{l_0} of 0.4, 0.8, 1.2, 1.5, and 1.8 at angles of β of 30° , 45° , 60° , and 70° and at values of σ from 0.50 to 1.50 are presented in figure 3 by using the data presented in reference 2. These curves all indicate that C_{d1} begins to rise rapidly at a C-factor of about 0.70 and that in the C-factor region from 0.75 to 0.80 the drag and, consequently, the loss has increased significantly. Hence, a simple pressure-recovery factor, the C-factor, was found to correlate the region of rapid drag rise (high loss region) independent of the various cascade parameters. The available cascade C_{d1} values were not converted to loss coefficients since the C-factor range which describes the region of high loss would not be significantly altered by such a conversion because the rate of change of C_{d1} with C-factor at the start of the region of high drag is considerably more rapid than the rate of change of mean-flow direction which is used to convert C_{d1} to loss coefficient.

It should be pointed out that the cascade conditions herein investigated always had their peak-velocity point near the leading edge. As a result, there is probably very little change in the boundary-layer shape at the start of the adverse gradient over the range of cascade conditions investigated. Therefore, it is reasonable to expect a rather narrow range of C-factors to define the separation of the boundary layer. For blades which have their peak point well back on the blades, for example, the A_2I_8b blades of reference 7 near design angle of attack, the level of C-factor which corresponds to the region of rapid drag rise may be lowered because (1) a more severe adverse pressure gradient will occur, and (2) the boundary-layer shape parameter at the start of the adverse pressure

gradient will be greater than that which occurs nearer the leading edge. The successful use of such a loading parameter will require analysis of sufficient data to establish limiting values for typical examples of different-shaped pressure distributions. Since all the data presented in this paper are for incompressible flow, the extension of this loading parameter to conditions above critical speed will require establishment of the limiting values of C-factor which occur when boundary-layer growth has been influenced by shock boundary-layer interaction effects. Once the effects on the limiting values of C-factor of boundary-layer thickness at the start of the pressure recovery and adverse pressure gradient are determined, an accurate estimation of the region of efficient performance for any cascade configuration for which estimations of the surface pressure distribution can be obtained either from tests or analytical means should be possible.

CORRELATION OF ROTOR-LOSS DATA AND C-FACTOR

Analysis of Incompressible Rotor Test Data

An analysis of the incompressible rotor test data presented in reference 4 for medium cambered NACA 65-($C_{l_0} A_{10}$)10 blade sections, which were tested over a wide range of inlet angles at solidities of 1.0 and 0.5, was undertaken to determine whether rotor losses and C-factors would correlate in the same manner as did the cascade data. The rotor was a free-vortex design (exit tangential velocity inversely proportional to the radius). It had constant solidity along the blade length, and solidity was changed by varying the number of blades.

Rotor C-factors were obtained by using the low-speed cascade data of reference 2 to determine the static pressure at the peak surface-velocity point for the appropriate cascade conditions, whereas the downstream static pressure was obtained from the rotor measurements. The use of cascade data to obtain blade-surface minimum static pressure is reasonable since good agreement between cascade and rotor pressure distributions was obtained at design angle of attack in reference 7, and this agreement should persist at higher than design angles of attack until flow separation in one element of the rotor influences the rest of the flow field.

Rotor-loss coefficients were obtained from the rotor test data by using the formula

$$\bar{w} = \frac{P_{2,r,i} - P_{2,r}}{P_{1,r} - P_1}$$

The radial stations selected for an evaluation of $\bar{\omega}$ and C-factor were the inboard section ($r = 11.26$ inches), the mean radius section ($r = 12.41$ inches), and the outboard section ($r = 13.56$ inches). The inboard and outboard stations were almost 12 percent span from the inner and outer casings, respectively, and were selected to be outside the wall boundary-layer region. However, the inboard section was later found in reference 4 to be somewhat engulfed in the hub boundary layer. The conditions evaluated were design-angle-of-attack conditions and above.

The following table lists the inlet angles which exist at the three radial stations under investigation when the mean radius section is at its design angle of attack for each of the blade-setting angles and the two solidities:

Mean radius blade-setting angle, ξ , deg	Inlet angle, β , deg; $\sigma = 1.0$ and 0.5		
	Inboard	Mean	Outboard
$\xi_d + 17.5$	68.0	70.0	71.5
$\xi_d + 7.5$	57.6	60.0	62.2
ξ_d	49.8	52.5	55.0
$\xi_d - 7.5$	42.2	45.0	47.5
$\xi_d - 15.0$	34.8	37.5	40.0

The values of ξ_d for the inboard, mean, and outboard stations are 34.7° , 40.0° , and 44.5° , respectively, at $\sigma = 1.0$ and are 39.0° , 44.3° , and 48.8° at $\sigma = 0.5$.

Figure 4 presents the variation in rotor-loss coefficient with C-factor for the various blade-setting angles. The vertical marks indicate design-angle-of-attack conditions. The evaluation was carried to the highest angle of attack for which the C-factor could be evaluated by using the cascade data to determine minimum suction surface static pressure. In some instances, the low-speed cascade data were extrapolated somewhat to obtain a minimum surface static-pressure value for the point where $\bar{\omega}$ began to rise. The highest angle-of-attack conditions that could be evaluated by using cascade data with some small amount of extrapolation were generally less than the rotor-surge angle of attack. Hence, rotor surge generally occurs at higher angles of attack than the high-drag region of the low-speed cascade data since the angles of attack for the cascade tests were almost always high enough to include the region of rapid drag rise.

From figure 4, the following results can be observed:

(1) At the mean radius section (the section closest to being in a two-dimensional flow field), loss coefficient generally increased significantly for C-factors above 0.75. This observation is similar to the results observed in the cascade tests.

(2) Both inboard and outboard stations indicated a steady increase in loss coefficient with C-factor and a significant increase in loss coefficient at a lower C-factor level than occurred at the rotor mean radius section and in the cascade tunnel. At $C = 0.70$, the mean value of loss coefficient at the outboard and inboard stations was 0.05 and 0.10, respectively, at $\sigma = 1.0$, and was 0.09 for both stations at $\sigma = 0.5$, compared with 0.02 and 0.03 at the mean radius for $\sigma = 1.0$ and 0.5, respectively. This difference results between the performance of the more extreme stations and the mean radius station because, although the flow at the mean radius station is nearly two-dimensional, the flow at both inboard and outboard stations is strongly influenced by three-dimensional effects. The inboard station is influenced by the interaction of inner casing and blade boundary-layer flow, whereas the outboard station is influenced by both the effects of centrifuged blade boundary-layer flow and tip clearance.

The data presented in figure 4 correspond to rather wide ranges of inlet angle and, hence, angle of attack. For verification of this fact, see figure 5 (to be discussed in more detail in the next section) where the same rotor data used in figure 4 have been replotted with inlet angle rather than C-factor as the abscissa. Therefore, the variation of loss coefficient with C-factor was generally independent of inlet angle and solidity for a wide range of inlet angles, angles of attack, and solidities at each radial station with the exception of the outboard section where a rise in \bar{w} at a somewhat lower value of C-factor occurred for the low (0.5) solidity tests. For example, at the outboard station, high loss of the order of 0.09 corresponded to C-factors from 0.74 to 0.79 at $\sigma = 1.0$ and from 0.67 to 0.71 at $\sigma = 0.5$. Hence, a solidity effect was observed at the outboard station where the effects of centrifuged blade boundary-layer and tip-clearance effects are all important. Evidently, the lower solidity condition cannot tolerate as high a blade-surface-pressure recovery in this region.

In summation, the C-factor appeared to be equally effective in defining the high loss region in both rotor and cascade tunnel with the proviso that, at inboard and outboard stations, where three-dimensional effects are more pronounced, high loss region occurred at C-factors closer to from 0.65 to 0.70 than to 0.75 or above as indicated at the rotor mean radius section and in the cascade tests.

The C-Factor as a Rotor-Stall Indicator

When a rotor surges, that is, when severe pulsating flow occurs, it is generally the hub or tip section that stalls first; therefore, these

sections are of prime importance for any rotor analysis aimed at the prediction of the onset of surge. The criterion used to determine which radial station would stall first was to determine, from figures 10 and 11 of reference 4, which station first exhibited a dropoff or leveling off in turning angle with increasing angle of attack as the rotor flow coefficient was reduced by throttling. An examination of the variations in turning angle with angle of attack for the low-speed rotor data presented in reference 4 indicated that as the rotor was throttled the tip section stalled first for all blade-setting-angle conditions except those corresponding to the highest blade-setting angle at each of the solidities ($\sigma = 1.0$ and 0.5). For the highest blade-setting-angle conditions at each solidity, the hub section stalled first.

During the rotor tests it was observed, both audibly and from an unsteadiness of the fluid in the manometer boards used for pressure measurement, that before surge occurred there was a large high-angle-of-attack region of rather unsteady flow for the two lower blade-setting-angle conditions. No such angle-of-attack region was noted for the higher blade-setting angles. This unsteadiness at the two lower blade-setting-angle conditions invariably occurred after the outboard station had exhibited a severe drop in turning angle with increasing angle of attack. The unsteady points, which occurred for the highest blade-setting condition at both solidities, correspond to conditions where the turning angle at the inboard station exhibited a dropoff with angle of attack. It is reasonable to presume that this unsteadiness indicated a partial stall condition in the rotor. It was assumed that partial stall first occurred when any radial station first exhibited a dropoff in turning angle with increasing angle of attack since this variation in turning angle occurs only when severe flow separation exists at that radial station.

As stated previously, the variation in $\bar{\omega}$ with inlet angle for each of the test blade-setting angles at the three radial stations under consideration is presented in figure 5. (Each curve thus indicates the variation in $\bar{\omega}$ with angle of attack for a particular blade-setting angle.) The tick marks indicate unsteady-flow test results. The dashed portion of the curves corresponds to the region where the turning angle first exhibits a leveling off and then a dropoff with increasing angle of attack. The higher inlet-angle (angle of attack) point of the dashed portion of the curve for each blade-setting angle is considered to be the condition where rotor stall has occurred and is indicated by a solid symbol. The dash-dot lines are lines of constant C-factor. It may be seen that at $\sigma = 1.0$ the values of C-factor which correspond to the occurrence of rotor stall, when rotor stall is initiated in the tip region, range from 0.75 to above 0.78, whereas at $\sigma = 0.5$ they range from 0.70 to approximately 0.74. For the highest blade-setting conditions (see results corresponding to $\beta_{m,d} = 70^\circ$, $\xi_d + 17.5^\circ$) where the hub section stalled first, the C-factors at which rotor stall occurred were approximately 0.78

for $\sigma = 1.0$ and 0.74 for $\sigma = 0.5$. Hence, for the rotor conditions examined in this report, C-factor appeared to be effective in estimating rotor stall. The region of rotor stall was defined by a narrow range of C-factors, evaluated at the radial station where rotor stall was first initiated, for a wide range of inlet-angle conditions at each solidity.

CORRELATION OF ROTOR-LOSS DATA AND D-FACTOR

Analysis of Incompressible Rotor Test Data

In order to compare the effectiveness of the D-factor of reference 1 with the C-factor both at design and for angles of attack above design over a wide range of inlet-angle and solidity conditions, the low-speed rotor-loss data (much of which were used to prepare fig. 4) were compared with the corresponding blade-section D-factors. It should be pointed out that D-factor was derived for design-angle-of-attack conditions only and, hence, may not be meaningful at off-design conditions.

For the design-angle-of-attack conditions, the mean radius section exhibited low loss (below 0.05) for design-point D-factors as high as 0.64 for a wide range of blade-setting angles corresponding to inlet angles β from 37° to 71° and solidities σ from 0.5 to 1.0. This result is in reasonable agreement with one of the conclusions of reference 1 in which a design D-factor limit of about 0.60 was proposed. At design-angle-of-attack conditions, the inboard section exhibited low loss (below 0.05) for D-factors up to 0.45 at $\sigma = 1.0$ and 0.54 at $\sigma = 0.50$. These inboard-station limits are lower than was indicated in reference 1 but probably result because, as stated previously, the inboard station is engulfed in the hub boundary layer.

The variation in outboard-station loss coefficient with D-factor for the many rotors examined in reference 1 was indicated in figure 10 of that reference by the region bound by dashed lines. This same variation is indicated by dashed lines on the outboard-station results presented in figure 6. At design-angle-of-attack conditions, the losses associated with D-factors of approximately 0.59 at $\sigma = 1.0$ and 0.52 at $\sigma = 0.5$ were less than the results presented in reference 1. This difference in limiting D-factor level may result because, unlike the incompressible results presented herein, the results of reference 1 could be affected by compressibility effects. Also, any difference in the magnitude of the tip clearance and the thickness of the blade boundary layer which is centrifuged toward the tip from the more inboard sections could affect the tip limiting D-factor level.

In summary, figure 6 indicates that, for D-factors at design angle of attack of the order of 0.60 at the mean radius station, low loss coefficient may be expected. The data presented herein further indicate that a higher than 0.45 D-factor limit appears reasonable for the outboard section at design angle of attack at both solidity conditions. The inboard-section data indicate low D-factor limits of 0.45 at $\sigma = 1.0$ to

0.55 at $\sigma = 0.5$, but this result is not very significant since the inboard station was in the wall boundary-layer region.

Figure 6 indicates that there is no effective correlation of \bar{w} and D-factor at angles of attack above design. This was to be expected since the D-factor was derived for the design-angle-of-attack condition and does not include the increase in pressure recovery which occurs along the blade suction surface as angle of attack is increased above design. For example, for the same D-factor, blade sections set for low design inlet-angle conditions must operate at angles of attack farther from design than when set for higher design inlet angles. Hence, at the same D-factor, the amount of pressure recovery on the suction surface will be greater for the low design inlet-angle condition because of the effect of angle of attack on peak surface velocity. Since it is the amount of pressure recovery which limits loading, the lower design inlet-angle conditions should show a rapid rise in loss coefficient with D-factor at a lower D-factor level than the high design inlet-angle conditions. This conclusion is corroborated in figure 6 where, for example, at the mean radius and for $\sigma = 1.0$, the $\beta_d = 37.5^\circ$ curve ($\xi_d - 15^\circ$ curve) indicates $\bar{w} = 0.10$ at $D = 0.56$, whereas at $\beta_d = 60^\circ$ (the $\xi_d + 7.5^\circ$ curve) $\bar{w} = 0.036$ at $D = 0.56$. Therefore, the use of D-factor as a loading limit for low loss operation should be restricted to conditions near design angle of attack.

The D-Factor as a Rotor-Stall Indicator

In order to determine the D-factor values when rotor stall first occurs, the rotor data used to prepare figure 6 have been reexamined by plotting D-factor against inlet angle for each of the test blade-setting angles and solidities at three radial stations. (See fig. 7.) (Each curve thus indicates the variation in \bar{w} with angle of attack for a particular blade-setting angle.) The diagonal tick marks correspond to unsteady-flow conditions. The highest β point for each curve corresponds to the last test before severe pulsating surge occurred and, as described in the previous section, the solid symbols indicate the occurrence of rotor stall. For rotor stall which is initiated at the outboard station (the more common condition), D-factors from 0.57 to 0.64 describe the occurrence of rotor stall at both solidities except for the lowest blade-setting-angle condition at $\sigma = 0.5$ which had a D-factor stall value of 0.51. For hub stall which occurred at the highest inlet-angle conditions for each of the two solidities, D-factors of 0.85 at $\sigma = 0.50$ and 0.81 at $\sigma = 1.0$ were obtained.

At the outboard station, D-factor rose rapidly in the region above the onset of rotor stall. This rapid rise is a result of the rapid reduction in discharge velocity which results when separation occurs. Under such conditions the D-factor is no longer a measure of blade pressure recovery since pressure recovery must either level off or drop off when separation occurs.

It was shown previously that D-factor and loss coefficient did not correlate independent of design inlet angle at off-design conditions because D-factor does not include the effects of off-design angles of attack. Nevertheless, the rotor tests analyzed herein did indicate that D-factor appeared to be effective as a rotor-stall indicator for rotor stall initiated in the tip region. Rotor stall occurred for outboard-station D-factors of 0.57 to 0.64 over a wide range of inlet-angle and solidity conditions with the exception of the lowest blade-setting-angle condition at $\sigma = 0.5$ where rotor stall occurred at $D = 0.51$.

COMPILATION OF LOW-SPEED CASCADE PEAK SURFACE-PRESSURE-COEFFICIENT DATA

In order to facilitate the calculation of C-factors without recourse to the low-speed cascade pressure distributions of reference 2, the variations in peak pressure coefficient on the suction surface (upper surface) with angle of attack are presented in figure 8 for solidities of 0.50, 0.75, 1.00, 1.25, and 1.50 for values of C_{l_0} of 0.4, 0.8, 1.2, 1.5, and 1.8 and inlet angles of 30° , 45° , 60° , and 70° . The ordinate and abscissa were selected so that lines of constant α can be drawn if desired to permit the data to be used as carpet plots.

CONCLUSIONS

The following conclusions may be drawn regarding the development of a simplified loading-limit parameter for the prediction of inefficient performance for NACA 65- $(C_{l_0} A_{10})_{10}$ blades in cascade and in the rotor for incompressible flow conditions:

1. A simple loading-limit parameter (referred to as the C-factor) based on low-speed cascade data has been determined and found adequate for predicting the region of high loss for blades in cascade and in the rotor.

2. At the mean radius section of the rotor, loss coefficient had increased significantly for C-factors above 0.75 for the wide range of inlet angle and solidity conditions tested. Practically identical results were obtained in the low-speed cascade tunnel for cambers ranging from 0.4 to 1.8, inlet angles from 30° to 70° , and solidities from 0.50 to 1.5.

3. At both the inboard and outboard stations of the rotor, loss coefficient increased more rapidly with C-factor than it did at the mean radius section of the rotor and in the cascade tunnel. The high loss region

occurred at C-factors ranging from 0.65 to 0.70 rather than from 0.75 to 0.80 indicated at the rotor mean radius section and in the cascade tests.

4. The variation of loss coefficient with C-factor was generally independent of inlet angle and solidity for a wide range of inlet angles, angles of attack, and solidities at each radial station. The outboard section, however, exhibits a rise in loss coefficient at a somewhat lower C-factor value in the low solidity tests ($\sigma = 0.5$).

5. For the rotor conditions examined in this report, C-factor appeared to be effective in estimating rotor stall since the region of rotor stall was defined by a narrow range of C-factors, evaluated at the radial station where rotor stall was first initiated, for a wide range of inlet-angle conditions at each solidity. ($C = 0.75$ to over 0.78 at $\sigma = 1.0$ and 0.70 to 0.74 at $\sigma = 0.5$).

6. An examination and application of the simple blade loading-limit parameter D-factor of NACA RM E53D01 to low-speed rotor data for a wide range of inlet angles and solidities indicated that good agreement was obtained between the limiting value of design-angle-of-attack D-factor proposed in that paper ($D = 0.60$) and that obtained from the rotor data analyzed herein at the mean radius station. The results herein obtained, however, did indicate (1) lower limits at the inboard station, probably because that station was somewhat engulfed by the hub boundary-layer region, and (2) a less rapid increase in loss with design-angle-of-attack D-factor at the outboard station than the D-factor report indicated.

7. The use of the D-factor to correlate losses or as a loading limit for low-loss operation should be restricted to conditions near design angle of attack, as might be expected since D-factor was derived for design-angle-of-attack conditions. Nevertheless, the rotor tests analyzed herein did indicate that D-factor appeared to be effective as a rotor-stall indicator for rotor stall initiated in the tip region.

Langley Aeronautical Laboratory,
National Advisory Committee for Aeronautics,
Langley Field, Va., November 29, 1954.

REFERENCES

1. Lieblein, Seymour, Schwenk, Francis C., and Broderick, Robert L.: Diffusion Factor for Estimating Losses and Limiting Blade Loadings in Axial-Flow-Compressor Blade Elements. NACA RM E53D01, 1953.
2. Herrig, L. Joseph, Emery, James C., and Erwin, John R.: Systematic Two-Dimensional Cascade Tests of NACA 65-Series Compressor Blades at Low Speeds. NACA RM L51G31, 1951.
3. Loftin, Laurence K., Jr., and Von Doenhoff, Albert E.: Exploratory Investigation at High and Low Subsonic Mach Numbers of Two Experimental 6-Percent-Thick Airfoil Sections Designed To Have High Maximum Lift Coefficients. NACA RM L51F06, 1951.
4. Ashby, George C., Jr.: Comparison of Low-Speed Rotor and Cascade Performance for Medium-Camber NACA 65- $(C_{l0}, A_{10})_{10}$ Compressor-Blade Sections Over a Wide Range of Rotor Blade-Setting Angles at Solidities of 1.0 and 0.5. NACA RM L54I13, 1954.
5. Von Doenhoff, Albert E., and Tetervin, Neal: Determination of General Relations for the Behavior of Turbulent Boundary Layers. NACA Rep. 772, 1943. (Supersedes NACA WR L-382.)
6. Howell, A. R.: Design of Axial Compressors. Lectures on the Development of the British Gas Turbine Jet Unit Published in War Emergency Issue No. 12 of the Institution of Mechanical Engineers. A.S.M.E. Reprint, Jan. 1947, pp. 452-462.
7. Westphal, Willard R., and Godwin, William R.: Comparison of NACA 65-Series Compressor-Blade Pressure Distributions and Performance in a Rotor and in Cascade. NACA RM L51H20, 1951.

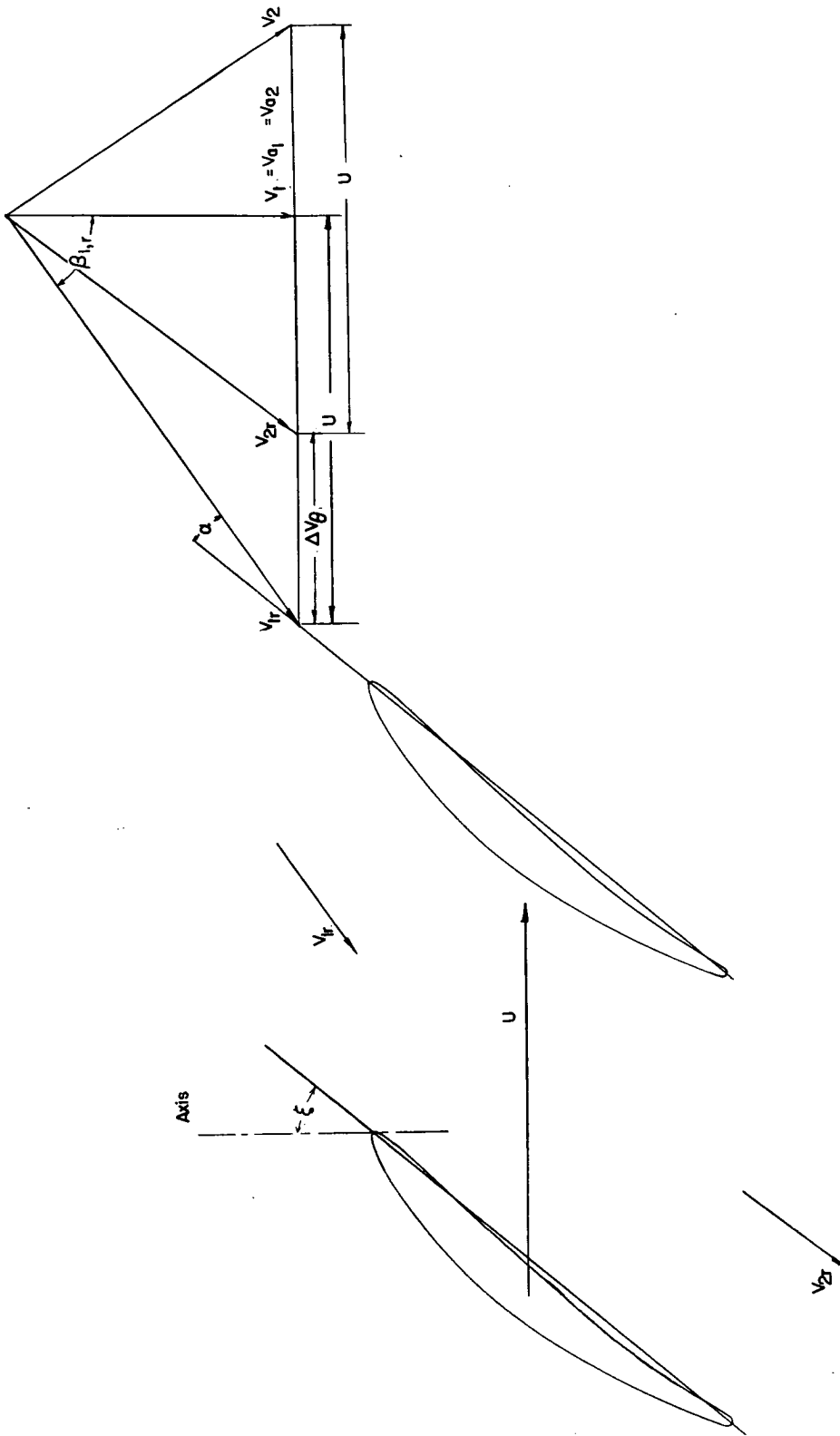
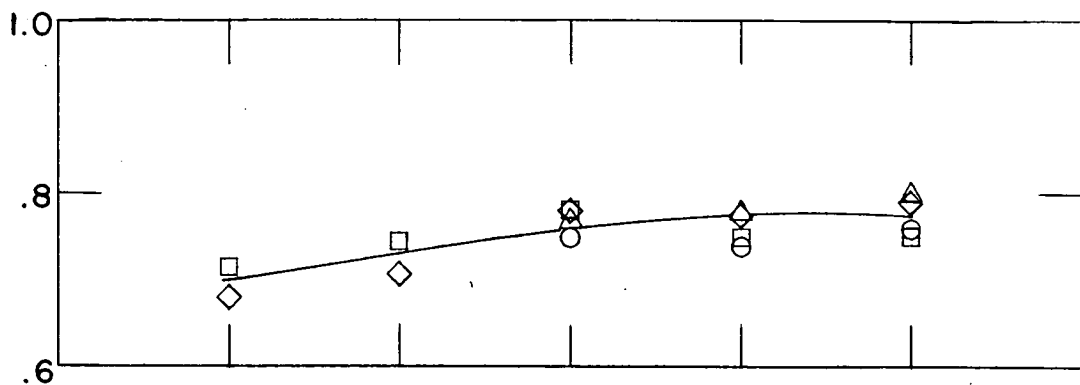
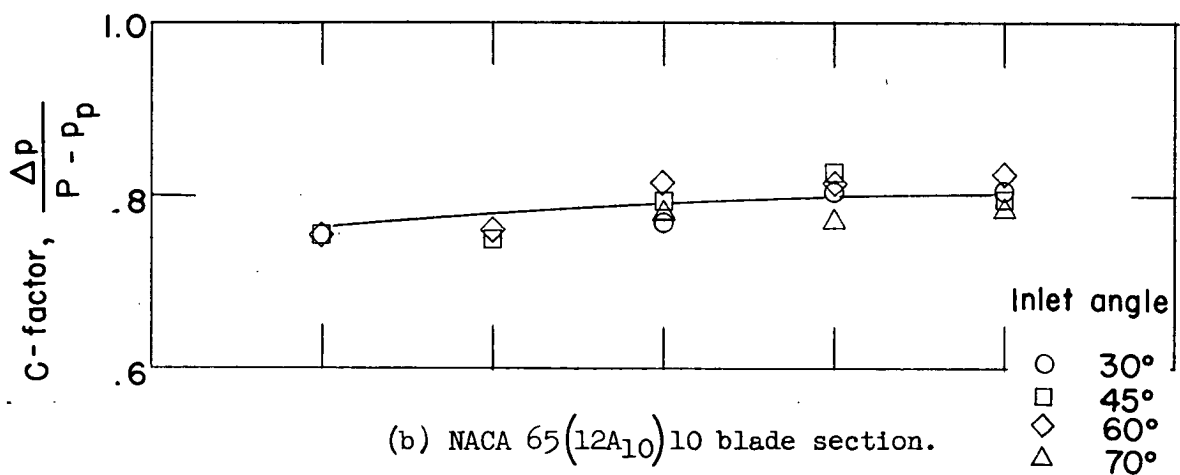


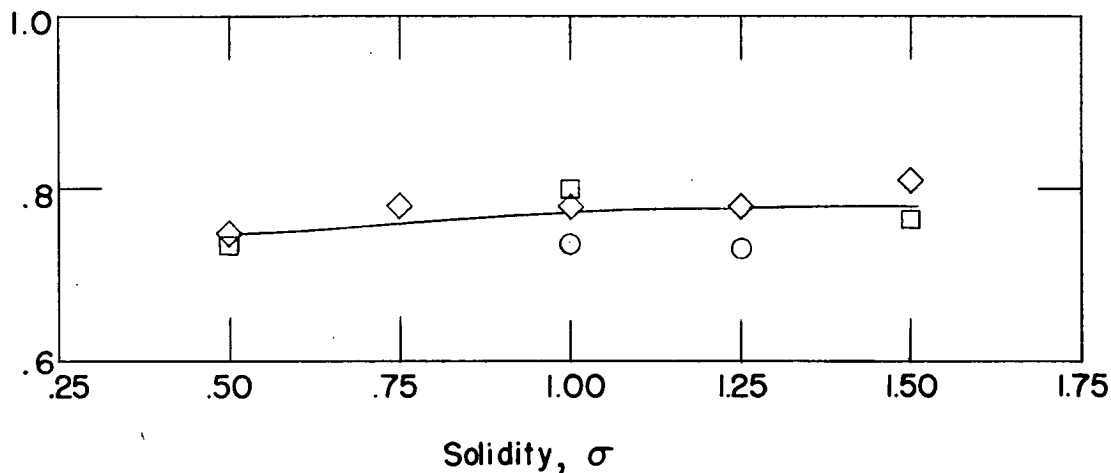
Figure 1.- Typical velocity diagram for rotor with no guide vanes and $V_{a1} = V_{a2}$.



(a) NACA 65(4A₁₀)10 blade section.



(b) NACA 65(12A₁₀)10 blade section.



(c) NACA 65(18A₁₀)10 blade section.

Figure 2.- Variation of C-factor, at twice minimum drag, with solidity for three blade sections in cascade at inlet angles from 30° to 70°.

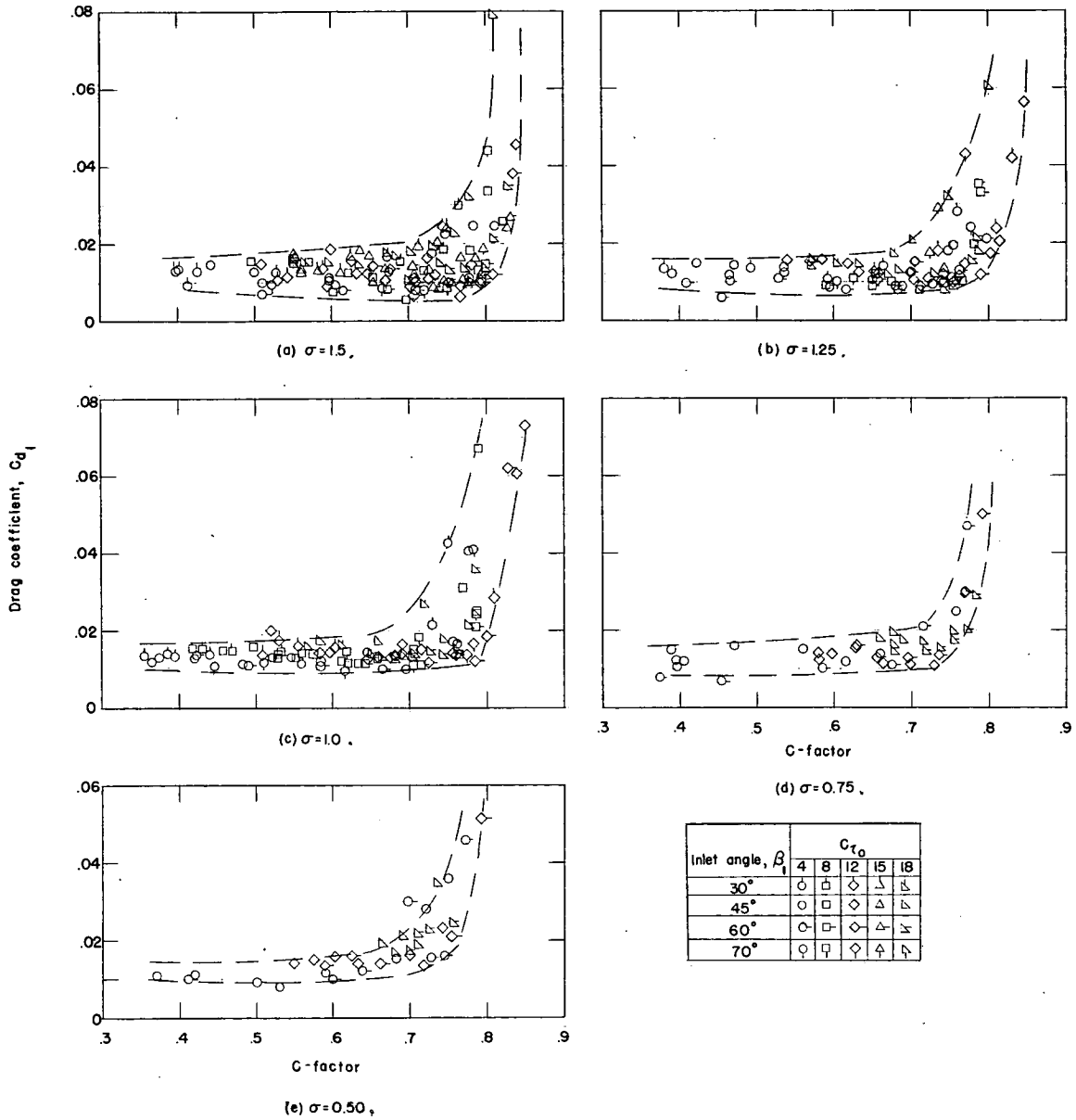
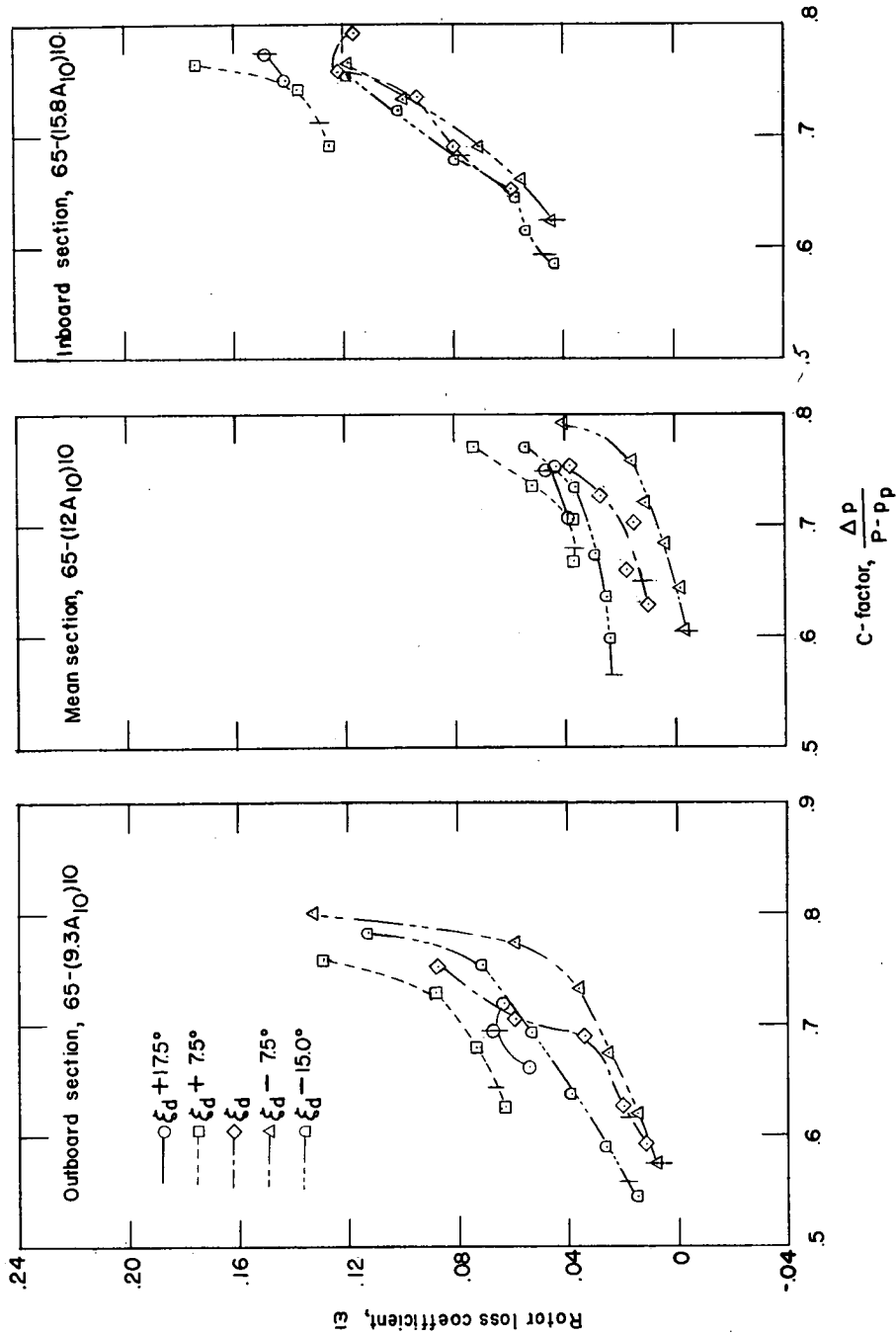
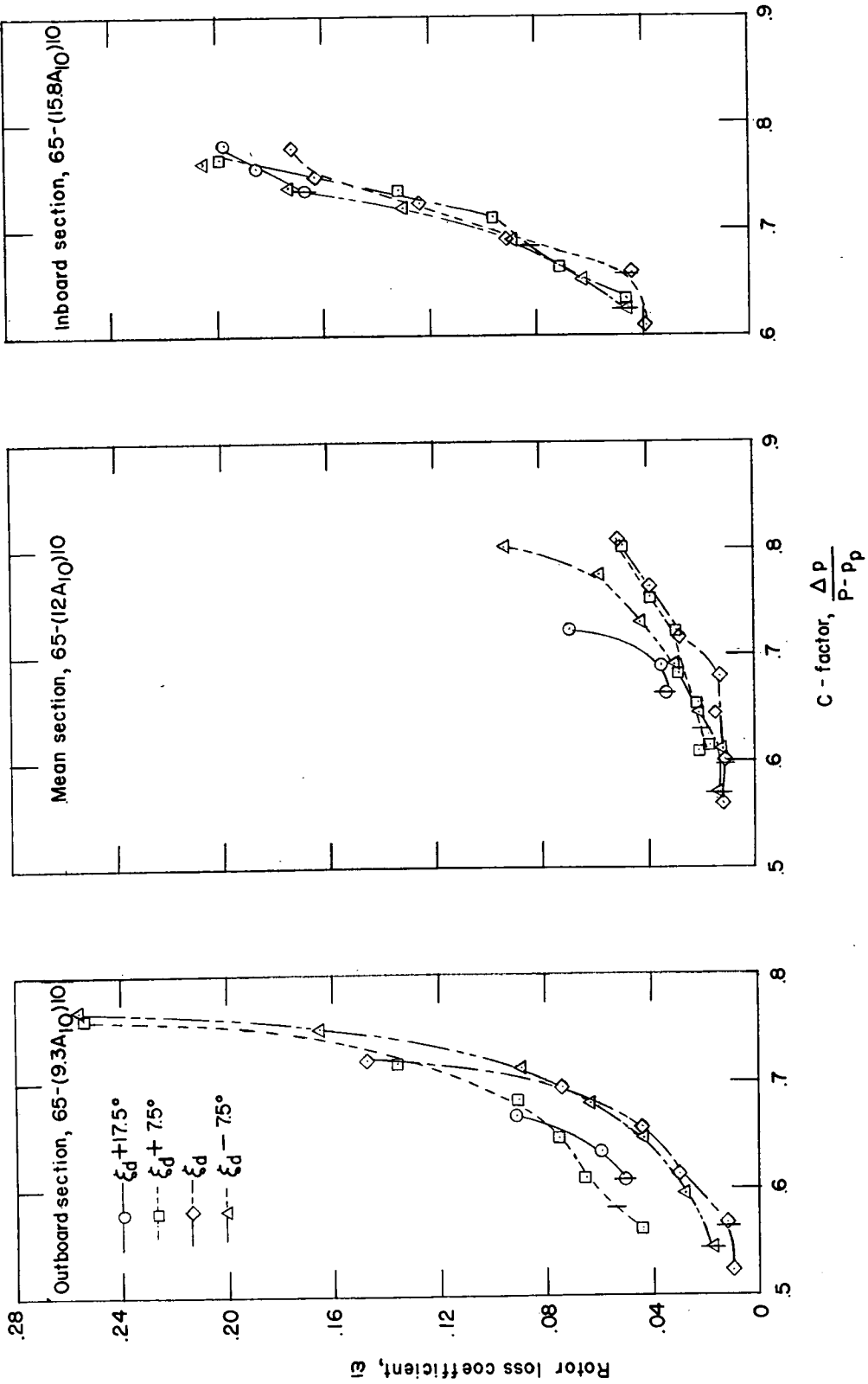


Figure 3.- Variation of drag coefficient with C-factor for angles of attack near design and above for NACA 65- $(C_{l_0}A_{10})_{10}$ blade sections in cascade having cambers from 0.4 to 1.8 at inlet angles ranging from 30° to 70° and solidities from 0.5 to 1.5.



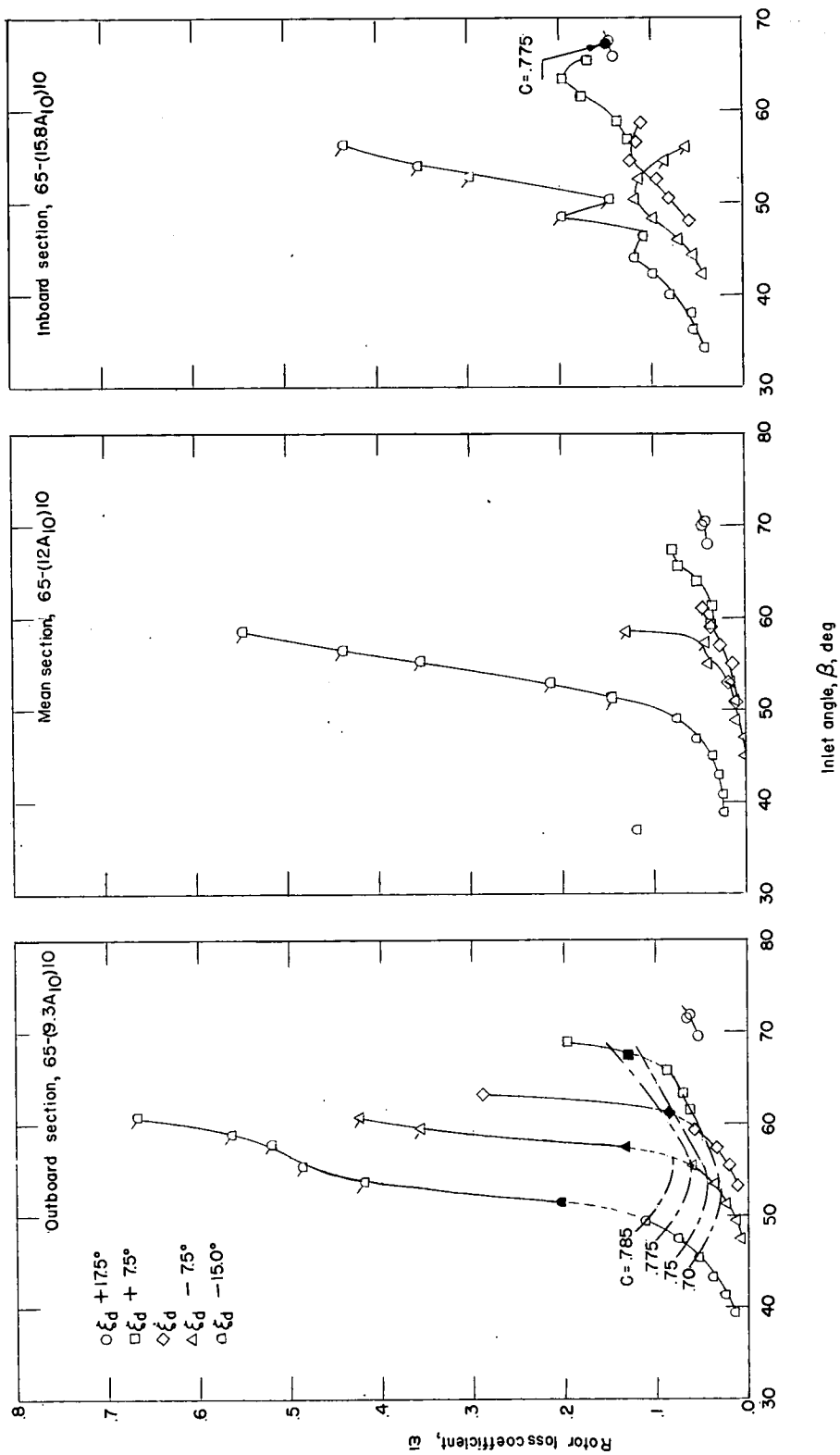
(a) $\sigma = 1.0$.

Figure 4.- Variation of rotor-loss coefficient with C-factor as angle of attack is increased above design for several rotor blade-setting angles at three radial stations. Vertical marks across curves indicate design-angle-of-attack conditions.



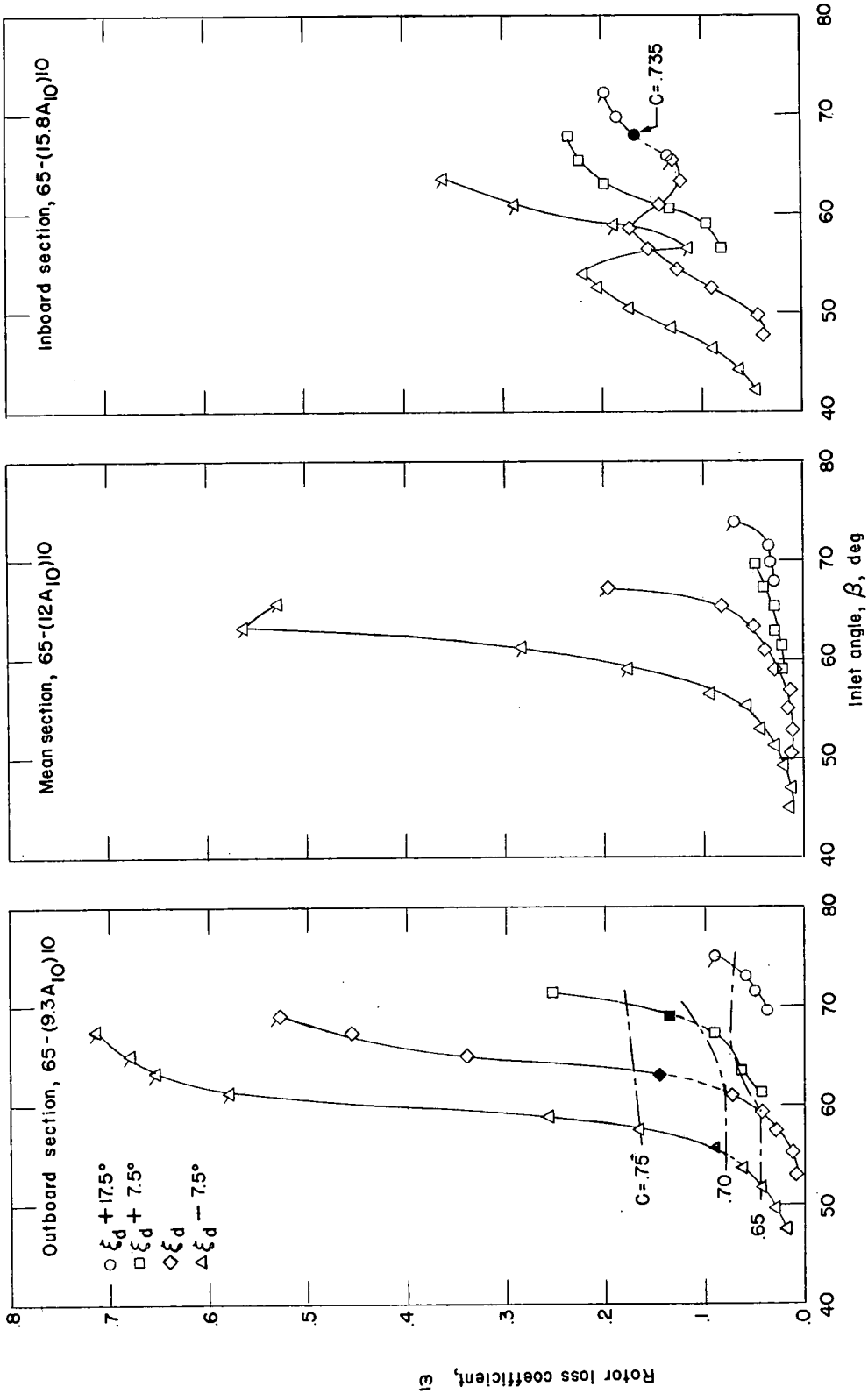
(b) $\sigma = 0.5$.

Figure 4.- Concluded.

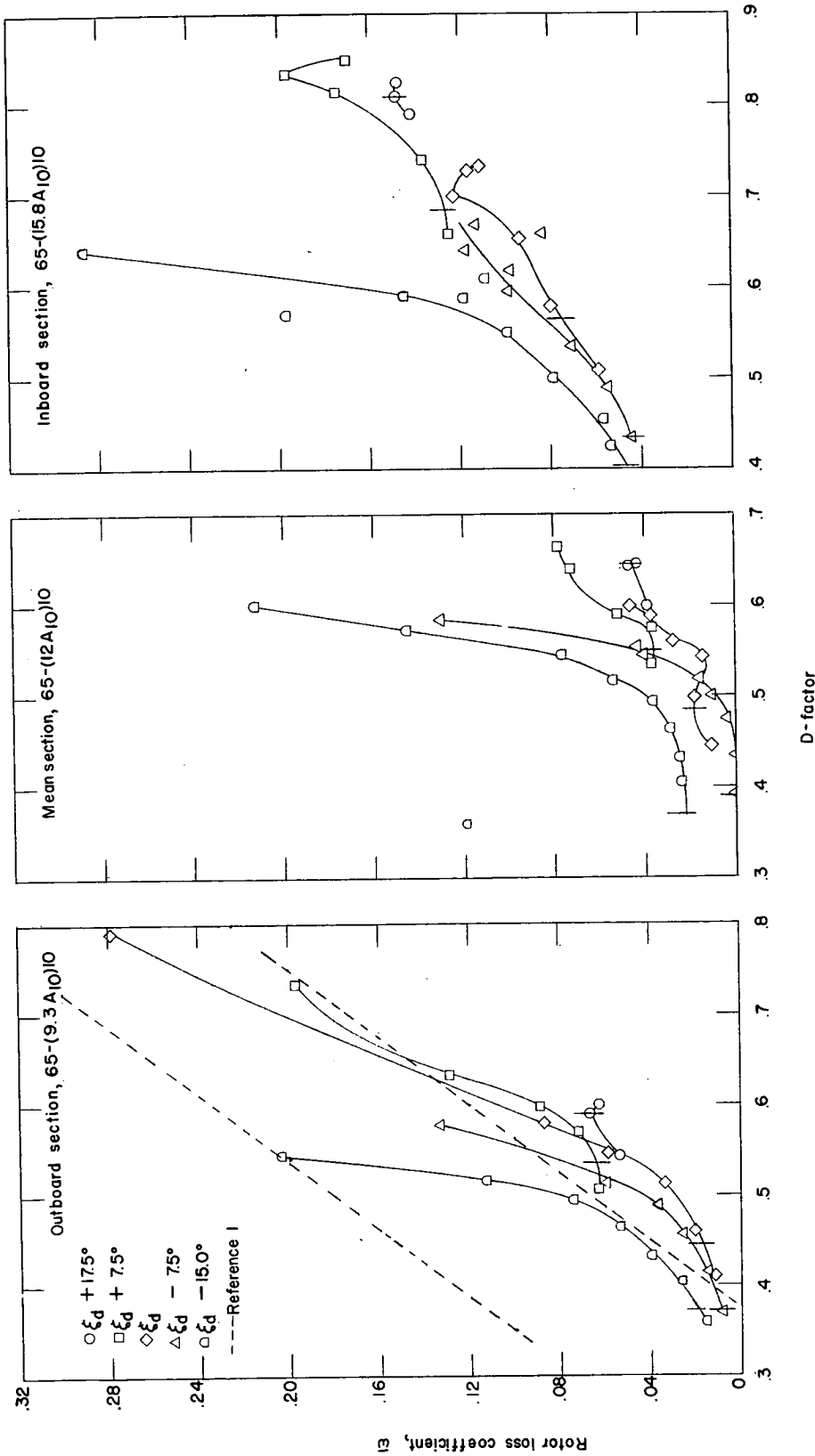


(a) $\sigma = 1.0$.

Figure 5.- Variation of loss coefficient with inlet air angle at each of the rotor blade-setting angles. The tick marks indicate the points in the high angle-of-attack region in which flow unsteadiness was noted.

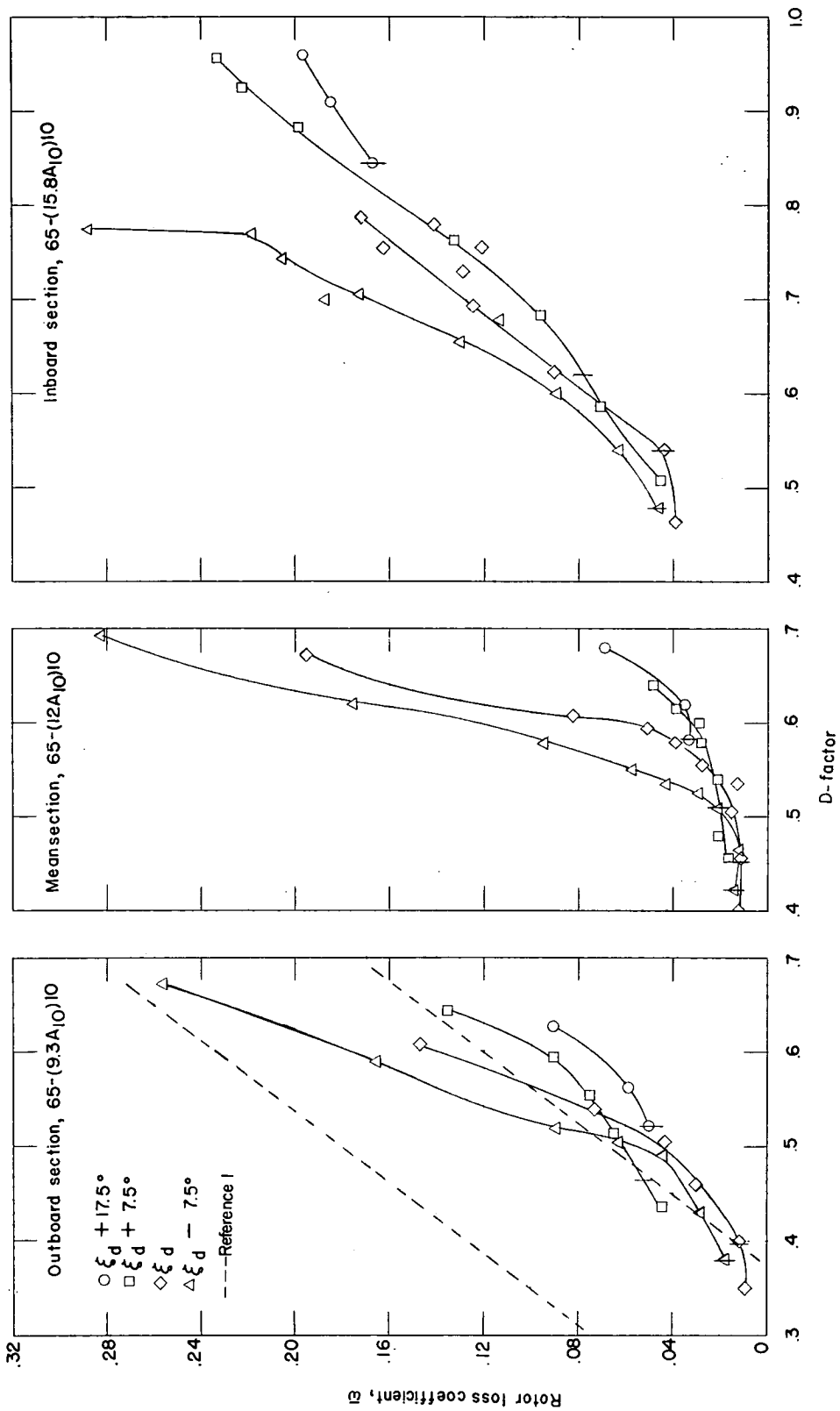


(b) $\sigma = 0.5$.
Figure 5.- Concluded.



(a) $\sigma = 1.0$.

Figure 6.- Variation of rotor loss coefficient with D-factor as angle of attack is increased above design for several rotor blade-setting angles at three radial stations. Vertical tick marks indicate design-angle-of-attack condition at mean radius section.



(b) $\sigma = 0.5$.
Figure 6.- Concluded.

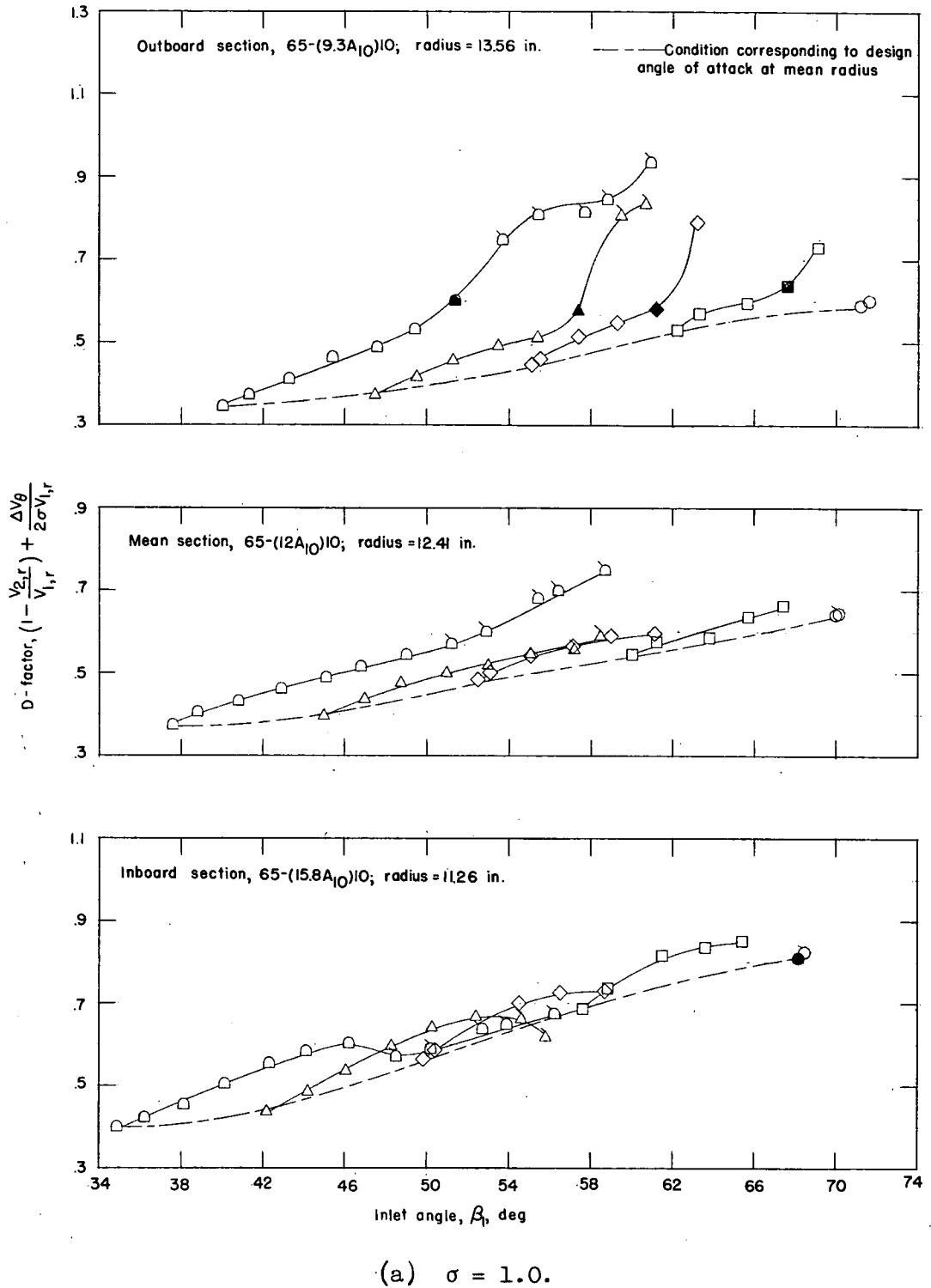
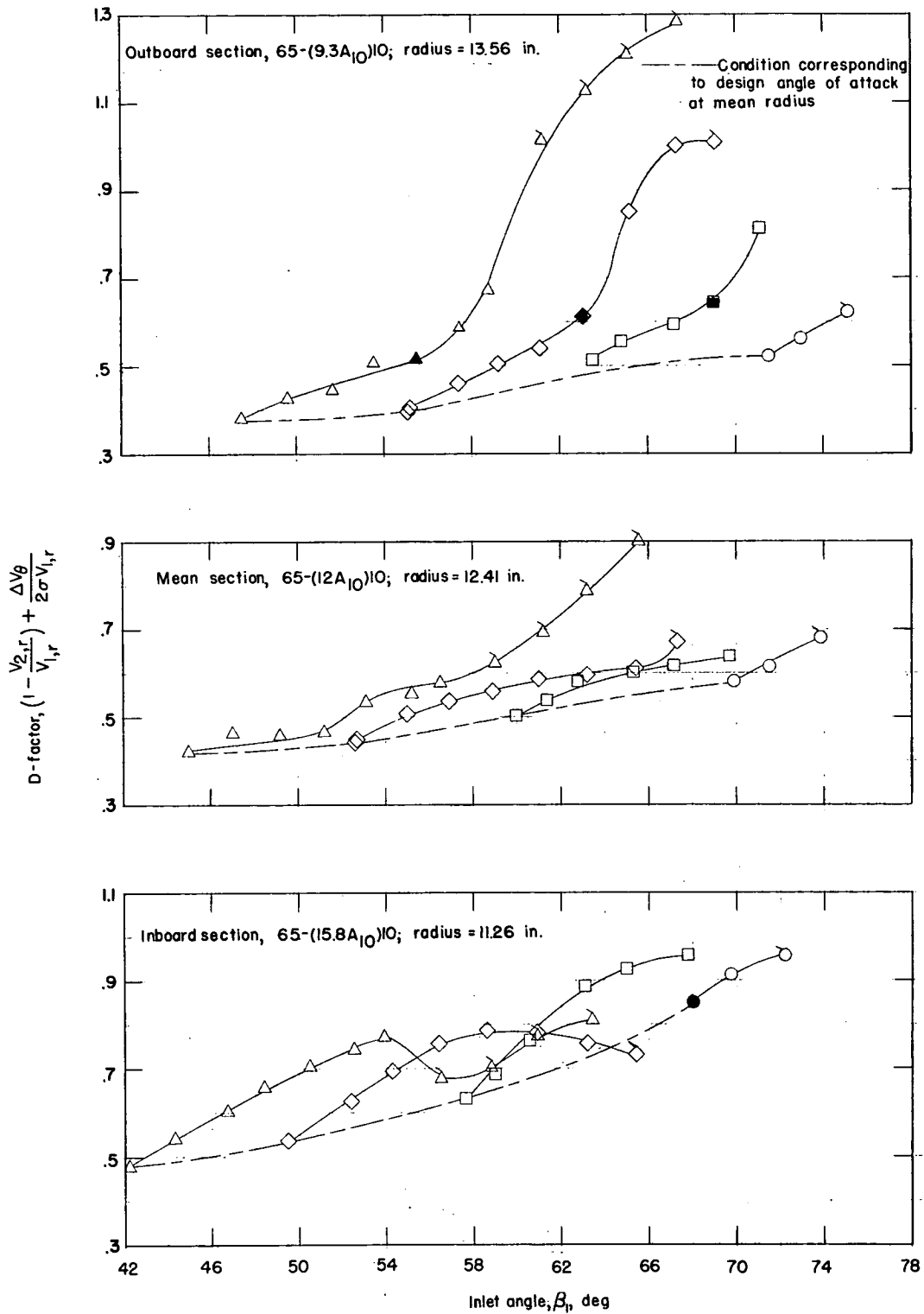


Figure 7.- Variation of rotor D-factor with inlet angle for several rotor blade-setting angles at three radial stations. The ticked symbols indicate test conditions where flow unsteadiness was noted.



(b) $\sigma = 0.5$.

Figure 7.- Concluded.

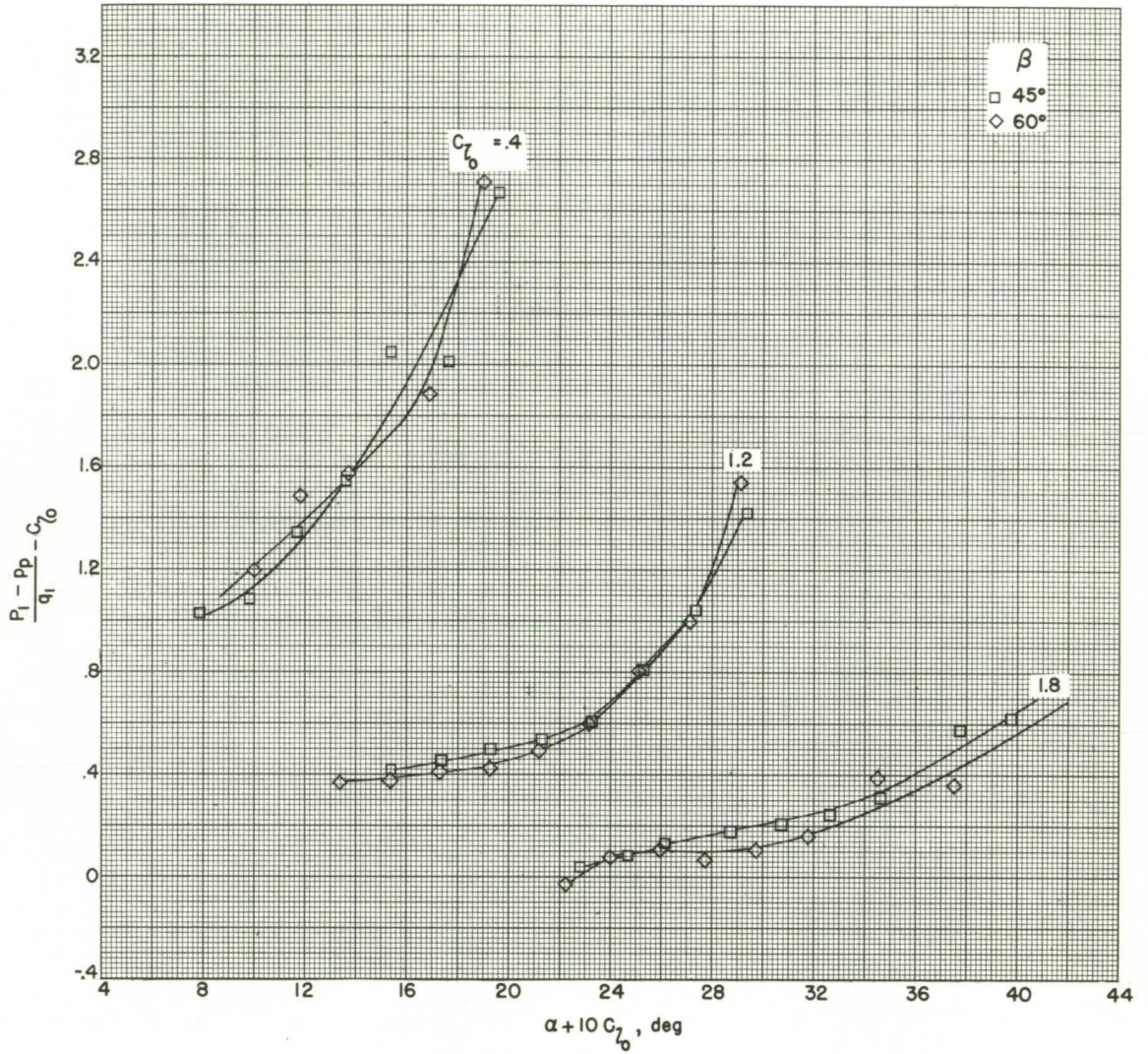
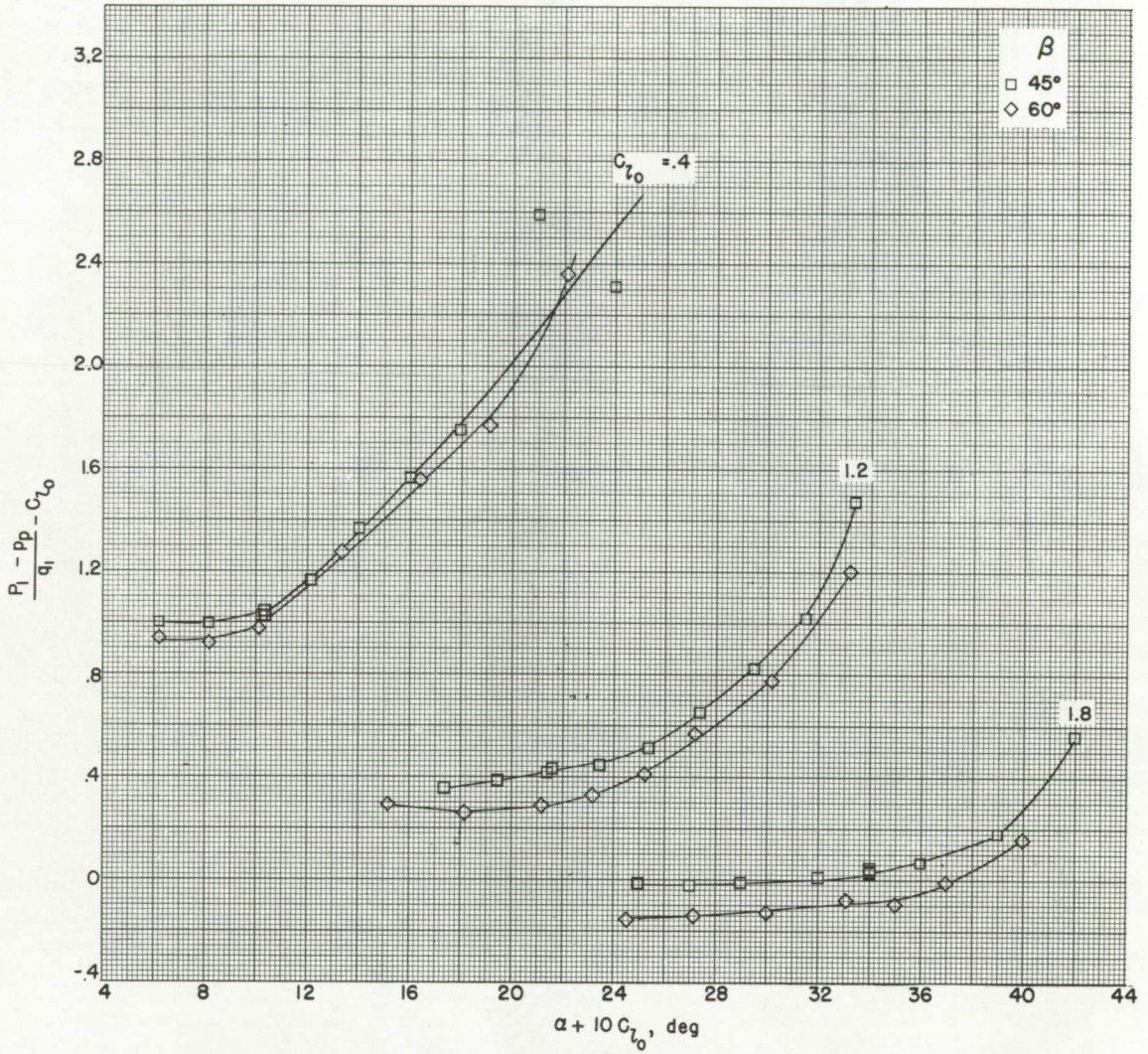
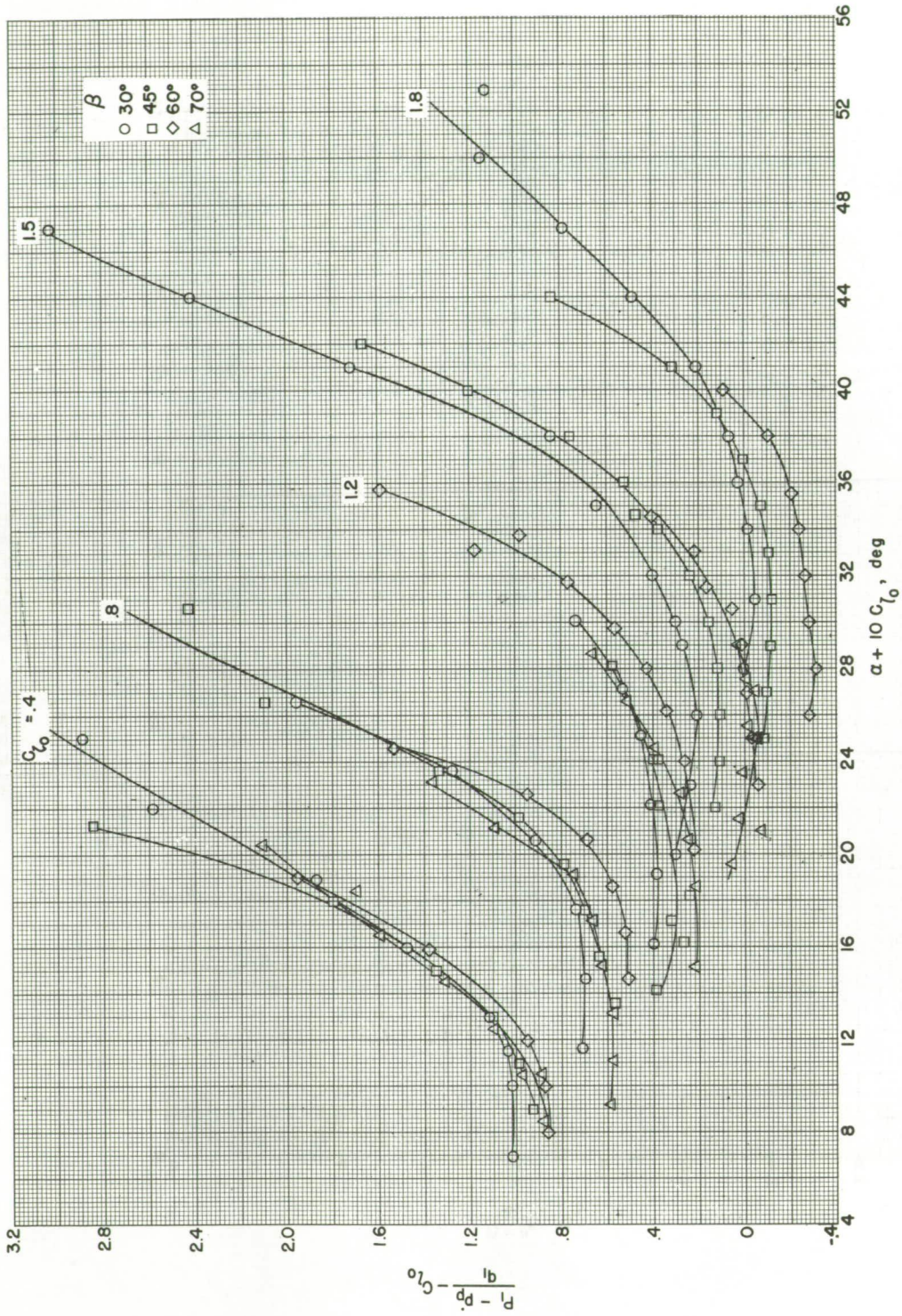
(a) $\sigma = 0.50$.

Figure 8.- Variation in low-speed peak pressure coefficient on the blade suction surface with angle of attack for various cambers and inlet angles.



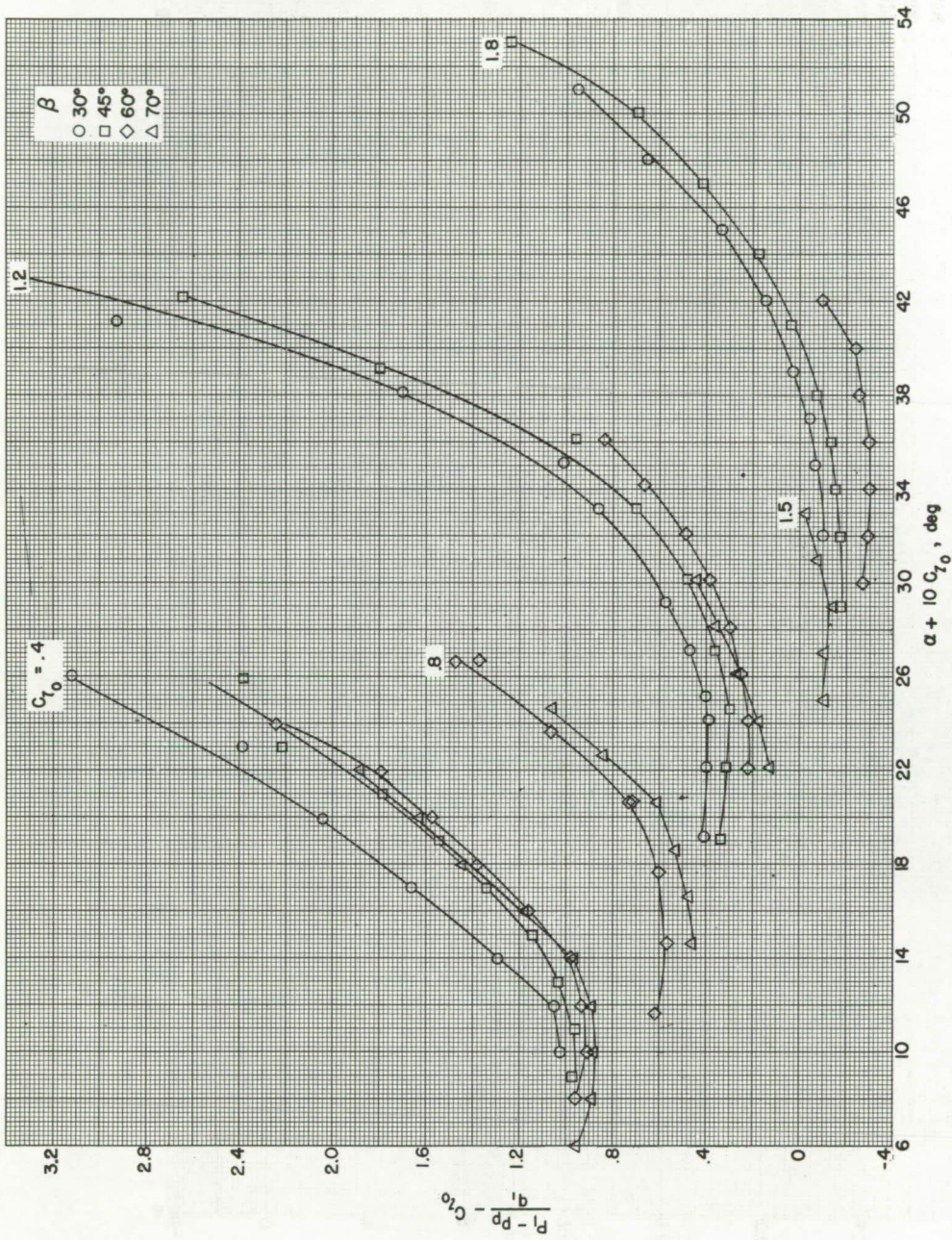
(b) $\sigma = 0.75$.

Figure 8.- Continued.



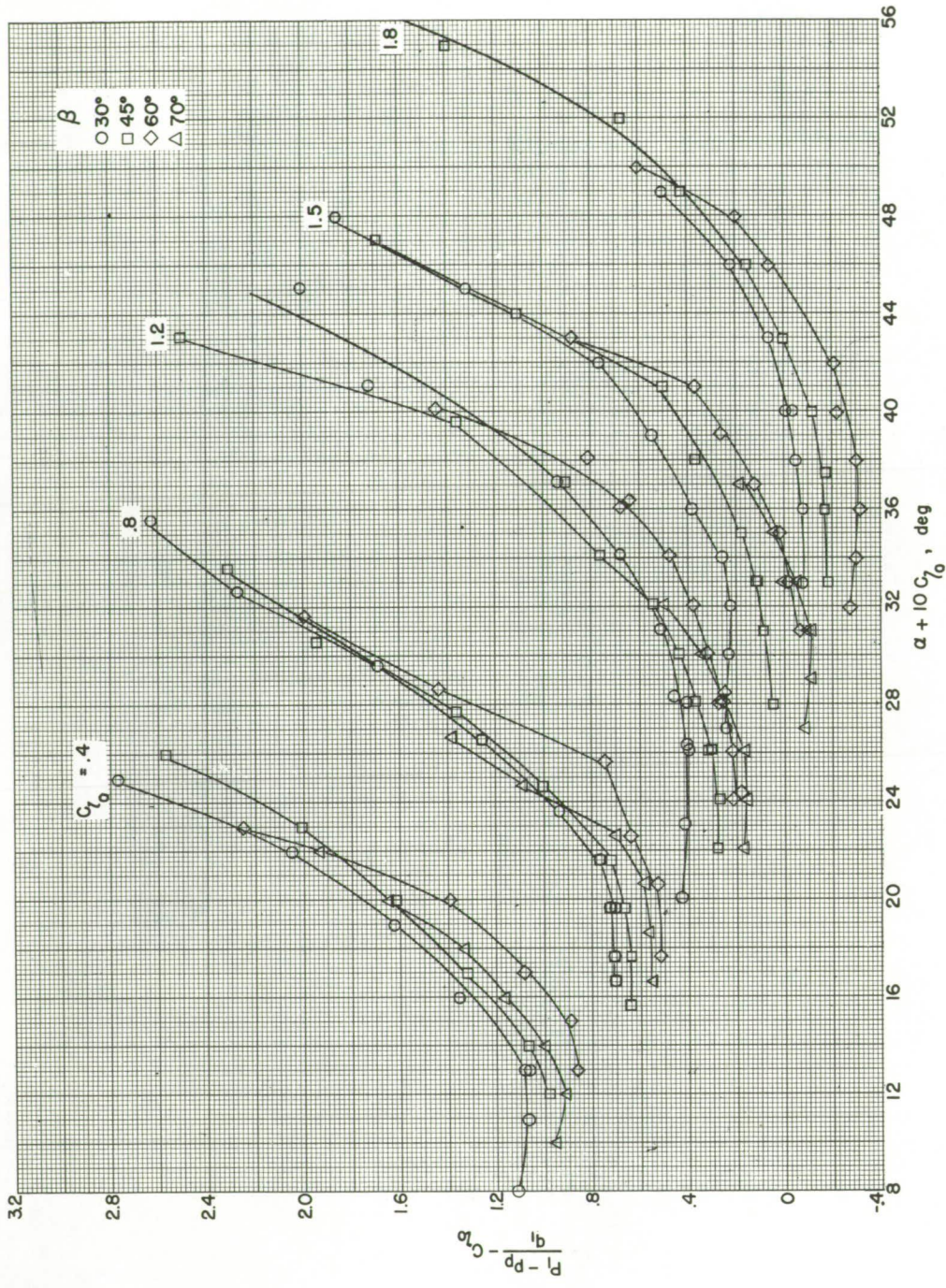
(c) $\sigma = 1.00$.

Figure 8.- Continued.



(d) $\sigma = 1.25$.

Figure 8.- Continued.



(e) $\sigma = 1.50$.

Figure 8.- Concluded.